Supplementary Information

Highly active heterogeneous Fe-based catalyst synergistically enhanced by polyaniline and MoS_2 for organic contaminants elimination

ChengBo Qian[a], Yuyuan Yao[a,b,*], Hongliang Zhu[c,*]

[a]National Engineering Lab of Textile Fiber Materials & Processing Technology (Zhejiang), Zhejiang Sci-Tech University, Hangzhou 310018, PR China

[b]Zhejiang Provincial Innovation Center of Advanced Textile Technology, Shaoxing 312000, PR China

[c]School of Materials Science and Engineering, Zhejiang Sci-Tech University, Hangzhou 310018, PR China

*Corresponding Authors: Y. Yao (E-mail: yyy0571@126.com), H. Zhu (E-mail: zhuhl@zstu.edu.cn).

Text S1. Experimental procedures

Carbamazepine (CBZ) was selected as a target contaminant for systematic evaluation of the catalytic performance of PANI-FeMoS$_2$. Degradation experiments were carried out in a 100 mL conical flask in which 20 mL CBZ solution (100 μM) and 4 mg catalysts were homogeneously mixed in the conical flask. The conical flask was placed in a shaker at a speed of 150 rpm while 200 μL PMS (0.1 M) was added and the chronograph was started. At the specified time intervals, 1.5 mL of the reactive solution was taken out and filtered through a syringe filter with 0.22 μm MCE membrane, which was injected into the 2 mL glass bottle containing 20 μL AA (0.01 M), and the concentration of residual CBZ was detected by ultrahigh performance liquid chromatograph (UPLC).

Text S2. Kinetics analysis

The reaction rate was calculated by a pseudo-first-order kinetics model (Eq S1) and the contaminants removal rate and the k-value were expressed as Eq S2 and Eq S3 respectively.

$$\ln (C_0/C_t) = k_{obs} \cdot t \qquad \text{Eq S1}$$

$$\text{removal rate} = (C_0 - C_t) / C_0 \times 100\% \qquad \text{Eq S2}$$

$$\text{k-value} = k_{obs} \times C_0 / (C_c \times C_p) \qquad \text{Eq S3}$$

where C_0 was the initial concentration of contaminants, C_t referred to the concentration at a certain time t during the catalytic reaction process, C_c and C_p represented the concentration of catalyst and PMS, respectively. The apparent reaction constant k_{obs} was evaluated from the slopes of plot of $-\ln (C_t/C_0)$ versus time.

Text S3. Characterization methods

The morphology of as-prepared samples was examined by Scanning electronic microscopy (SEM, FEI Scios 2 HiVac, USA) and Energy-dispersive X-ray spectroscopy (EDS, FEI Scios 2 HiVac, USA). Transmission electronic microscopy (TEM) was recorded on a Thermo Fisher Talos F200X G2 (USA). The lattice fringe of the sample was analyzed by Gatan Digital Micrograph software. The surface area and pore volume results were obtained by Brunauer-Emmett-Teller (BET) using Micromeritics ASAP 2460 (USA) at 77 K nitrogen. Fourier transform infrared spectroscopy (FT-IR) was performed on a Thermo Fisher Scientific Nicolet iS20 (USA). X-ray diffraction (XRD) were performed by a Rigaku Ultimate VI X-ray diffractometer (40 kV, 40 mA) by Cu Ka (λ=1.5406 Å) radiation. The Raman spectra were performed through using Horiba LabRAM HR Evolution (Japan) with the scan range from 50 cm^{-1} to 4000 cm^{-1} and a 532 nm excitation laser. X-ray photoelectron spectroscopy (XPS) was performed on Thermo Scientific K-Alpha (USA). Electrochemical Impedance Spectroscopy (EIS) were carried out in the CS2350M electrochemical workstation (Wuhan Corrtest Instrument Co., Ltd., China). Total organic carbon (TOC) removal of CBZ was determined by Jena Multi N/C 3100 (Germany). The electron paramagnetic resonance (EPR, Bruker EMX plus) spectra was employed to determine the ROSs. A SHIMADZU UV-2550 UV-vis spectrophotometer was used to record generation of the intermediate H_2O_2. Ultrahigh performance liquid chromatography (UPLC, ACQUITY UPLC H-Class PLUS) was used to determine the concentration of CBZ during the reaction process.

Text S4. Detection of H_2O_2

The potassium titanium sulfate coloration method was commonly used to detect the presence of H_2O_2 due to the reaction of H_2O_2 with titanium sulfate to produce a yellow deposit of the peroxide-titanium complex, which was dissoluble in strong acids, and the depth of the yellow coloration was linearly related to the concentration of hydrogen peroxide over a certain range. The concentration change of H_2O_2 can be known by detecting the absorbance at 400 nm.

Preparation of titanium sulfate reagent: 27.2 mL concentrated sulfuric acid was added to 30 mL deionized water, then 3.54 g potassium titanium oxalate ($K_2TiO(C_2O_4)_2$) was added, and finally the volume was fixed to 100 mL.

Experimental procedure: During the degradation of CBZ, 1.5 mL of reaction solution was added to a centrifuge tube containing 1.5 mL of titanium sulfate reagent at specific intervals, shaken vigorously to fully react, and finally poured into a clean cuvette to measure its absorbance at 400 nm by UV-vis spectrophotometer.

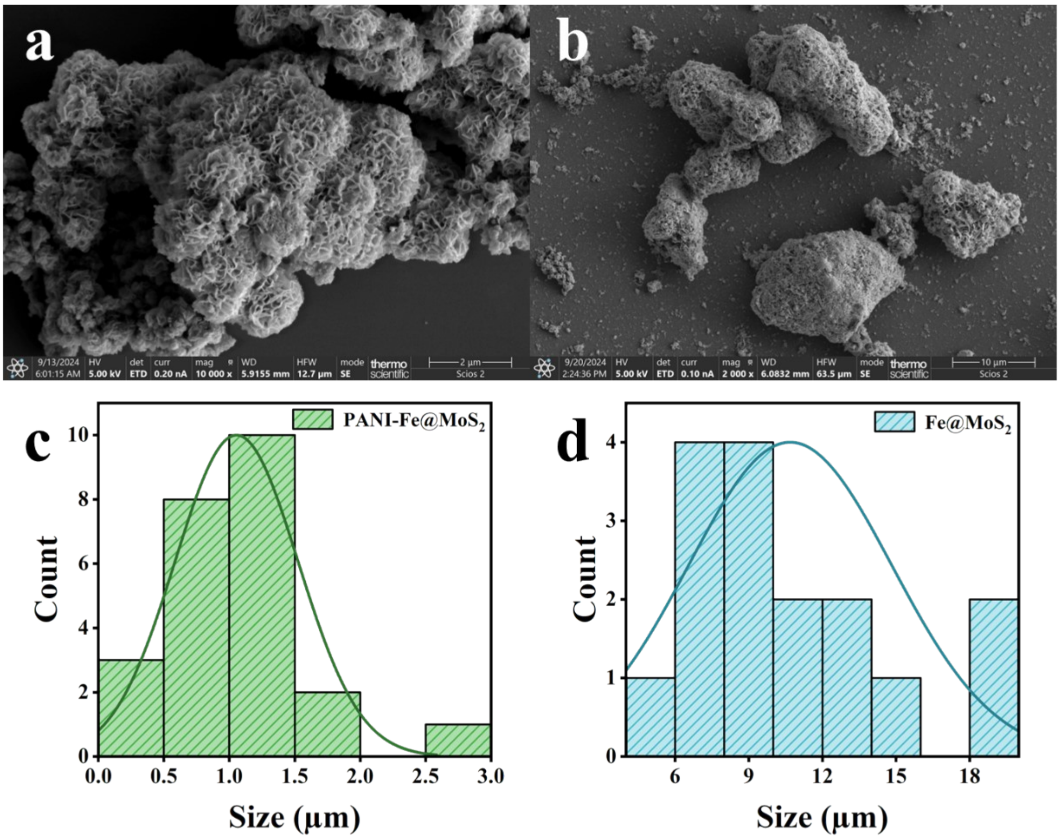

Fig. S1. The SEM images of (a) PANI-Fe@MoS$_2$, (b) Fe@MoS$_2$ and the corresponding particle size distribution maps of (c) PANI-Fe@MoS$_2$ and (d) Fe@MoS$_2$.

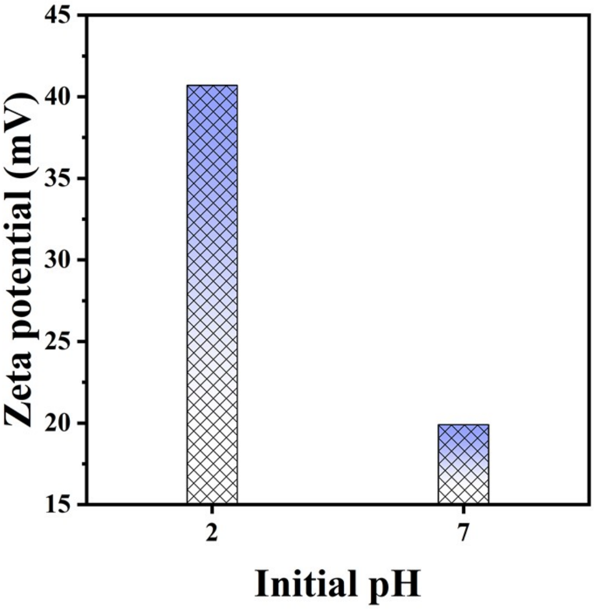

Fig. S2. Zeta potential of PANI at different initial pH.

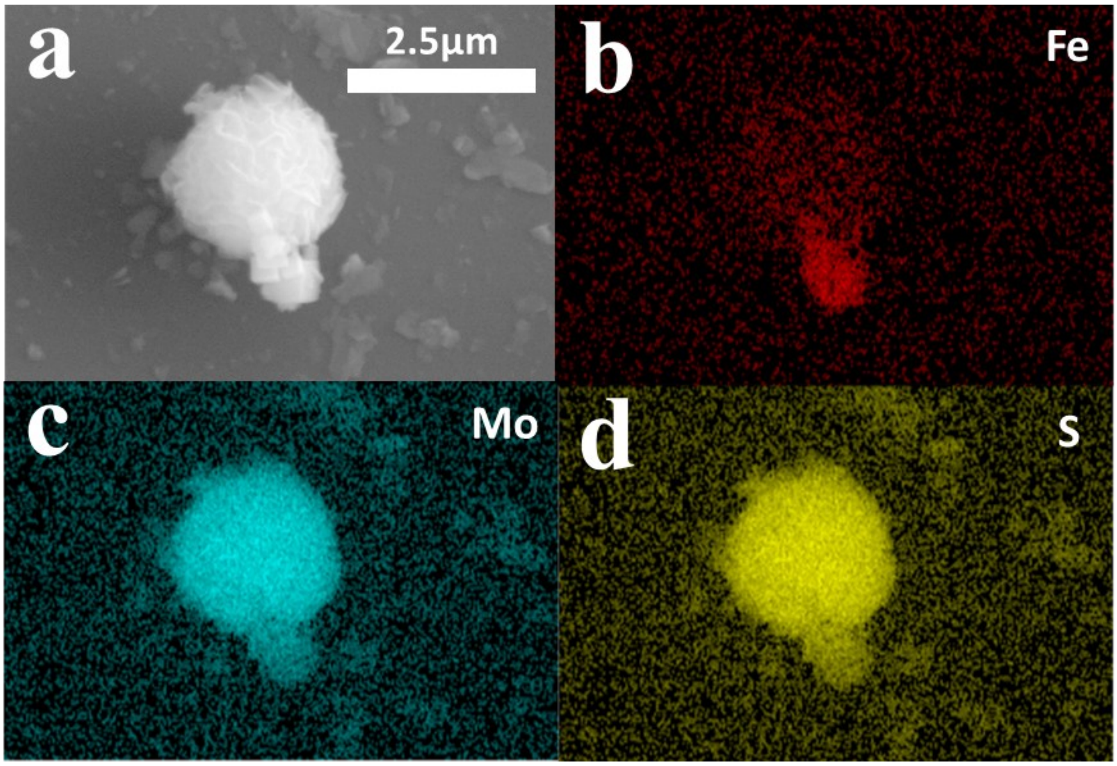

Fig. S3. (a) SEM images of Fe@MoS$_2$ corresponding to EDS elemental mapping images, (b-d) corresponding EDS mappings of Fe, Mo and S.

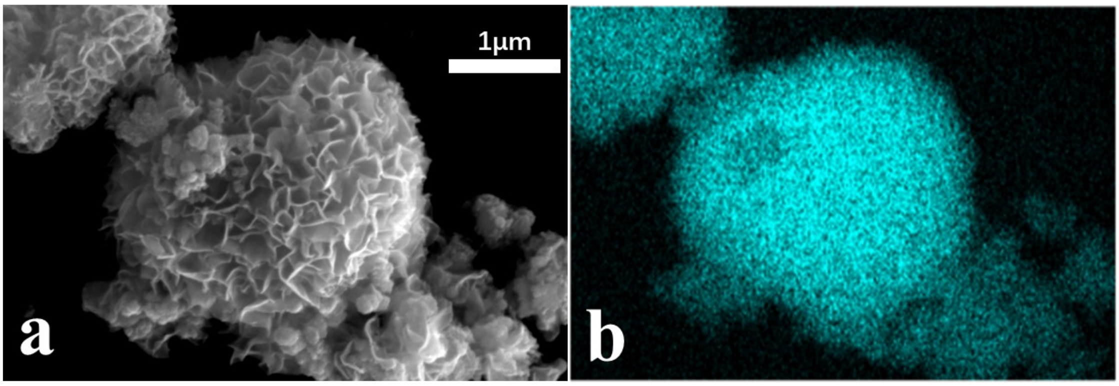

Fig. S4. (a) SEM images of PANI-Fe@MoS$_2$ and (b) corresponding to EDS mapping of S.

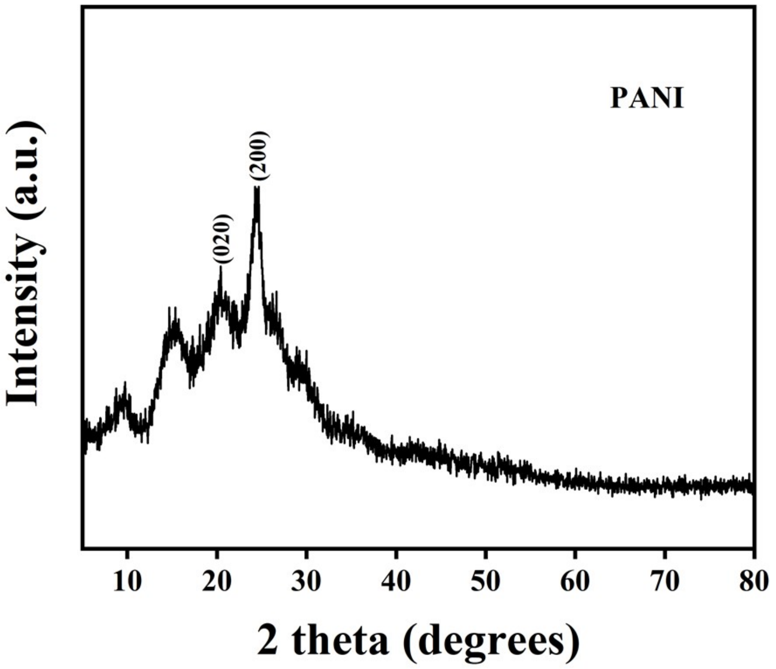

Fig. S5. XRD patterns of PANI. (The peak at 2θ = 15.2° was probably caused by the doping of HCI).

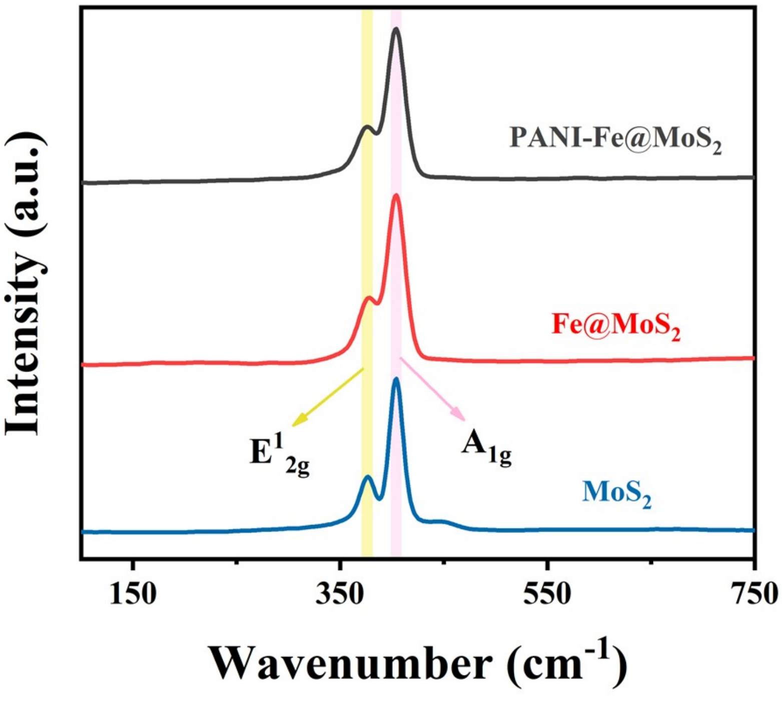

Fig. S6. Raman spectra of PANI-Fe@MoS$_2$, Fe@MoS$_2$ and MoS$_2$.

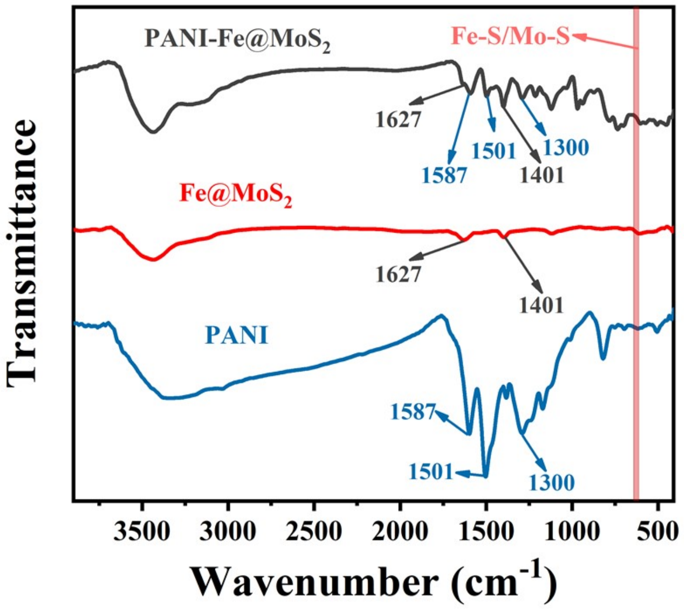

Fig. S7. FT-IR spectra of PANI-Fe@MoS$_2$, Fe@MoS$_2$ and PANI.

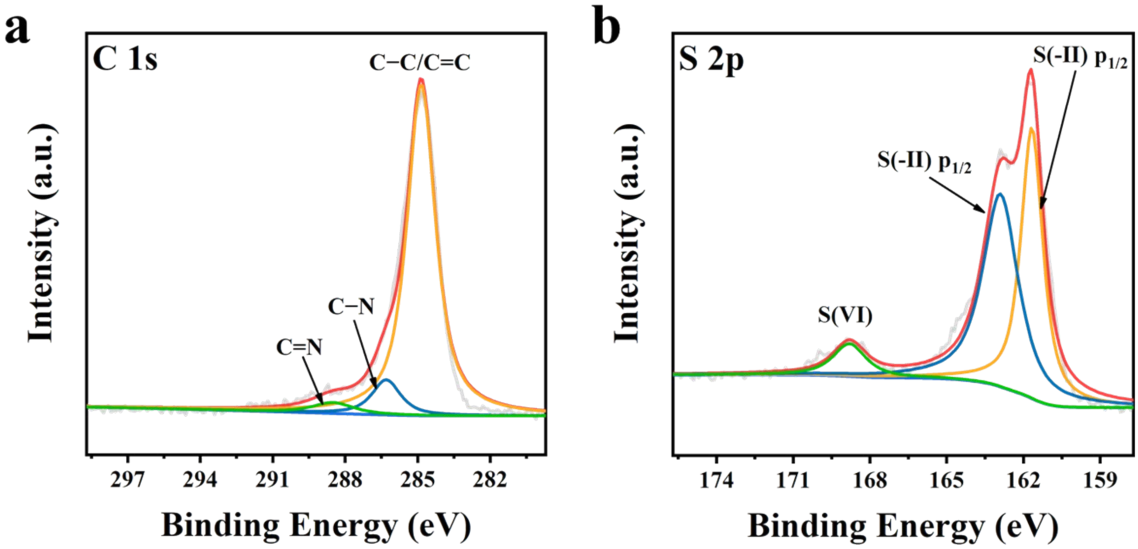

Fig. S8. (a) C 1s and (b) S 2p spectrum of PANI-Fe@MoS$_2$.

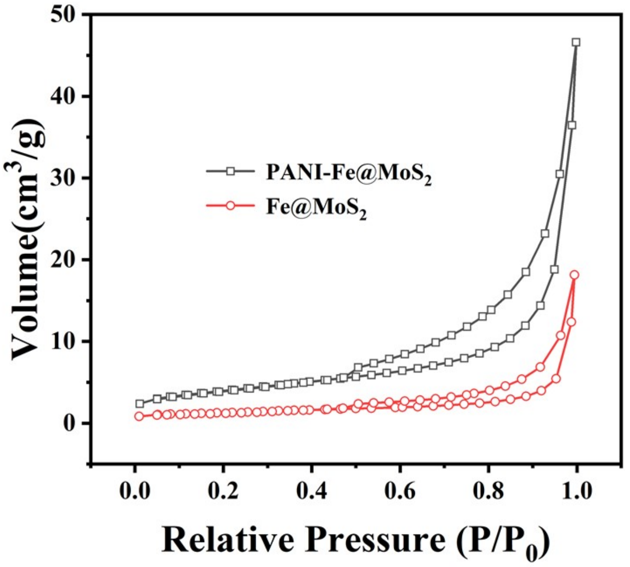

Fig. S9. Nitrogen adsorption desorption isotherm of PANI-Fe@MoS$_2$ and Fe@MoS$_2$.

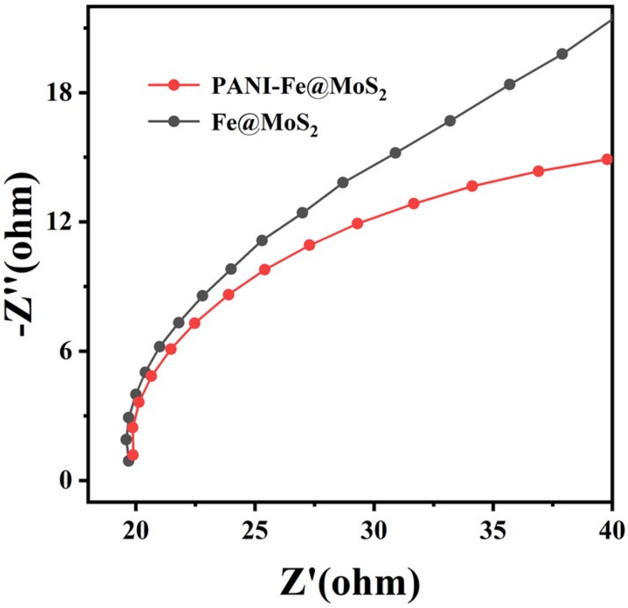

Fig. S10. Electrochemical impedance spectroscopy (EIS) Nyquist plot of PANI-Fe@MoS$_2$ and Fe@MoS$_2$.

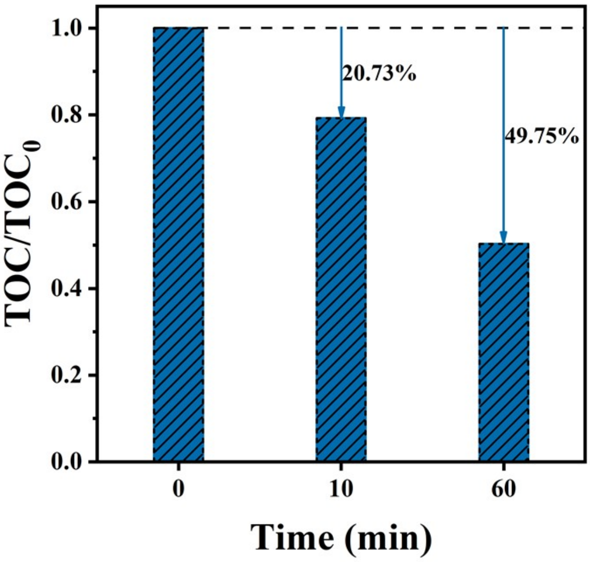

Fig. S11. The TOC removal at different times in the PANI-Fe@MoS$_2$/PMS system.

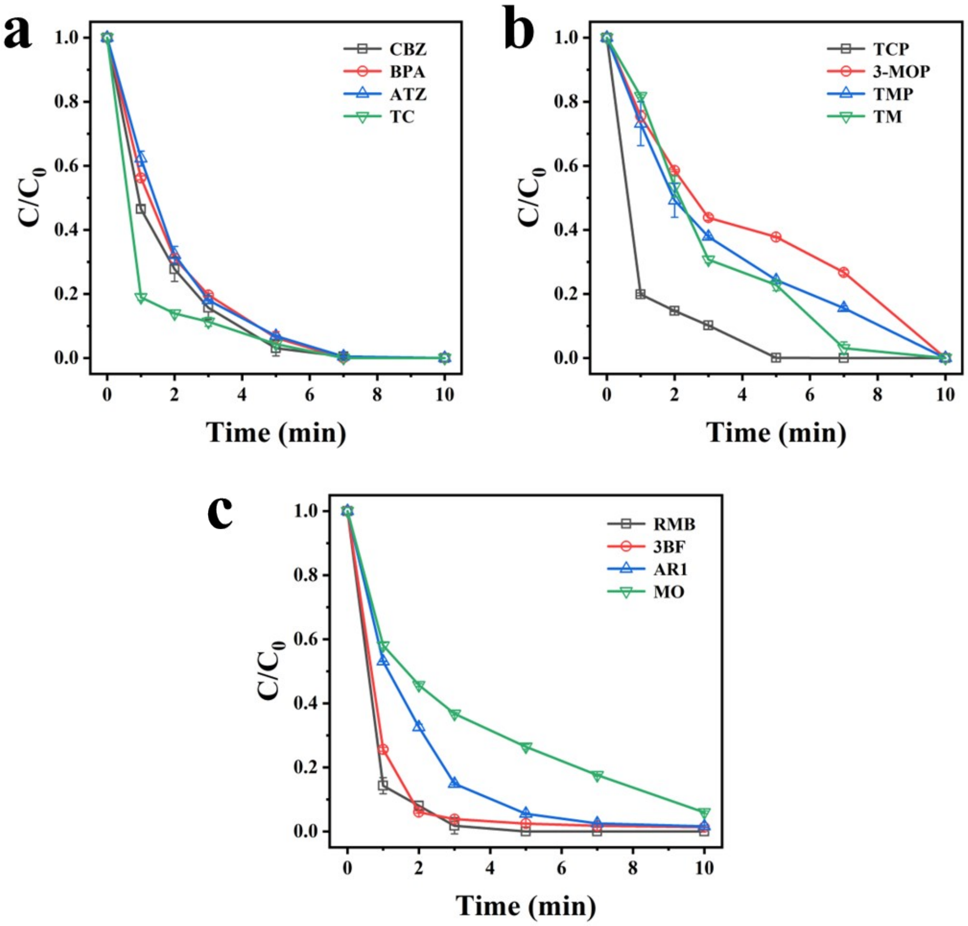

Fig. S12. Performance of PANI-Fe@MoS$_2$/PMS system for different organic pollutants.

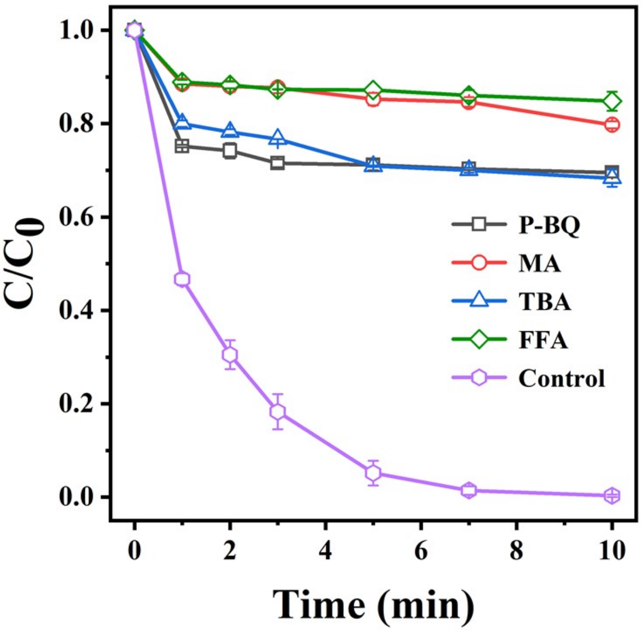

Fig. S13. The removal performance of the different scavengers.

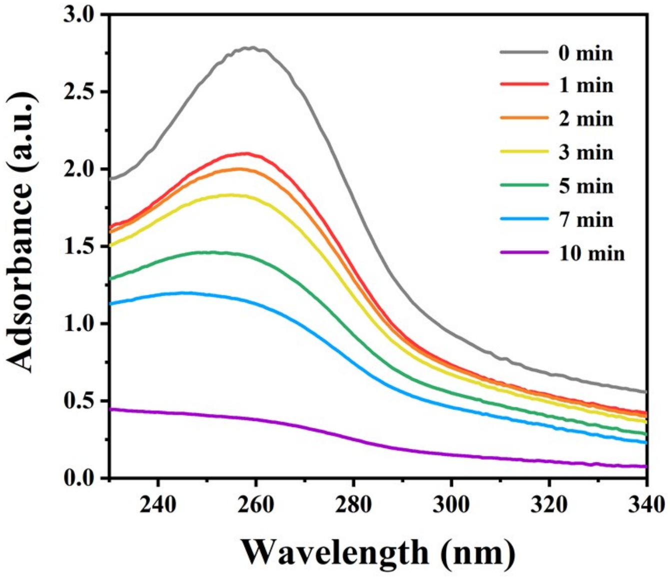

Fig. S14. The UV spectra of NBT in PANI-Fe@MoS$_2$/PMS system.

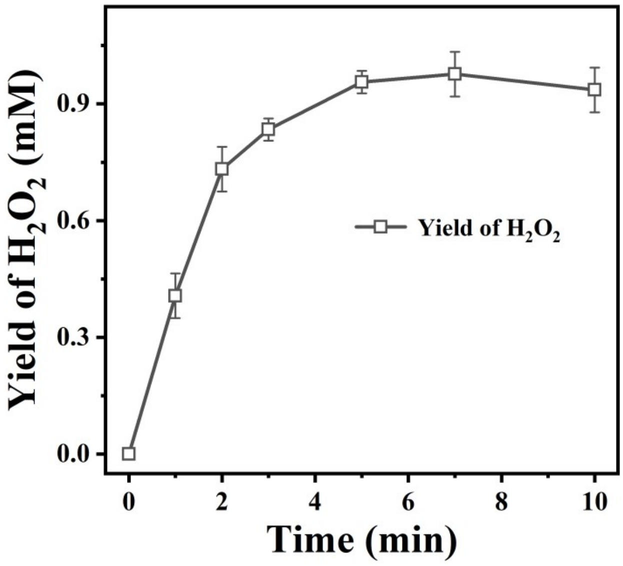

Fig. S15. The yield of H_2O_2 during the reaction.

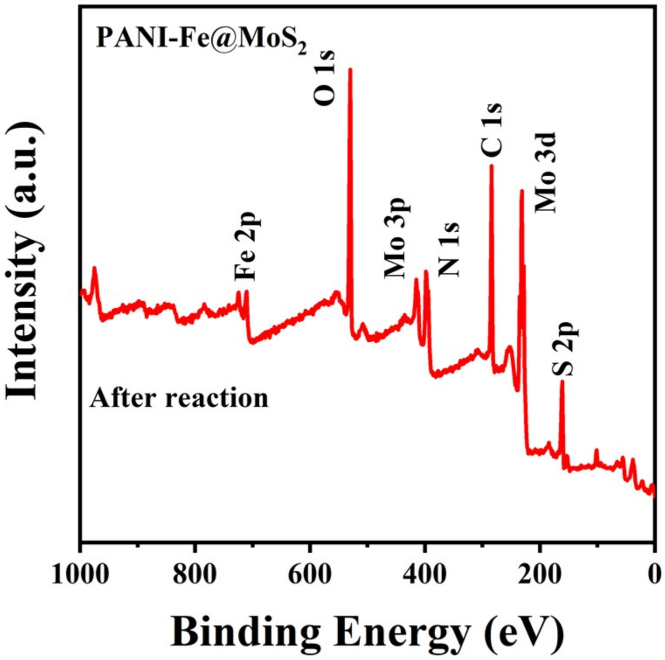

Fig. S16. The full XPS survey spectrum of PANI-Fe@MoS$_2$ after reaction.

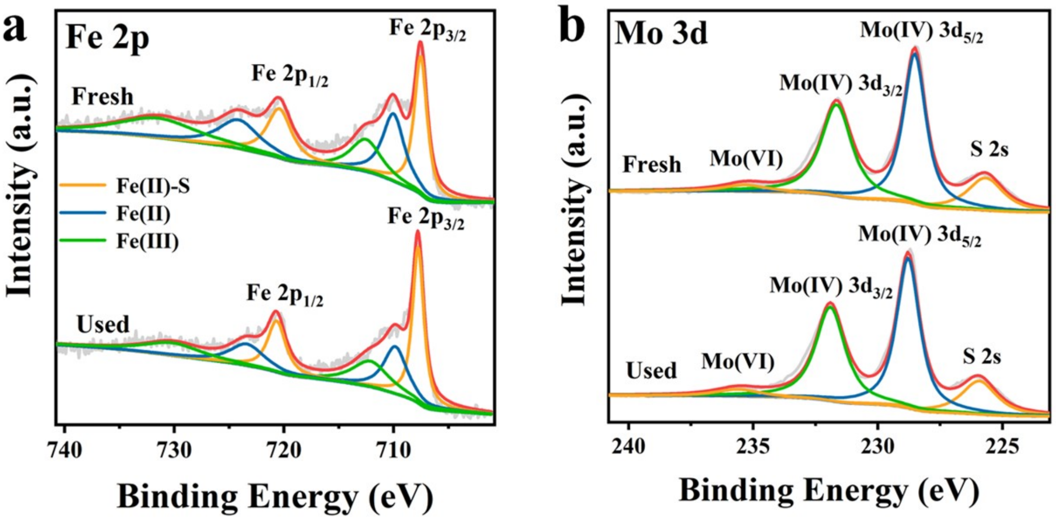

Fig. S17. (a) Fe 2p and (b) Mo 3d spectra of Fe@MoS_2 before and after the reaction.

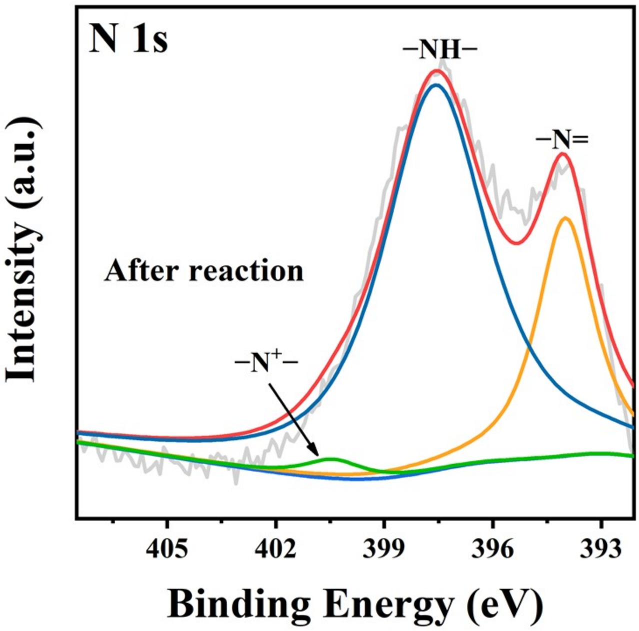

Fig. S18. N 1s spectra of PANI-Fe@MoS_2 after the reaction.

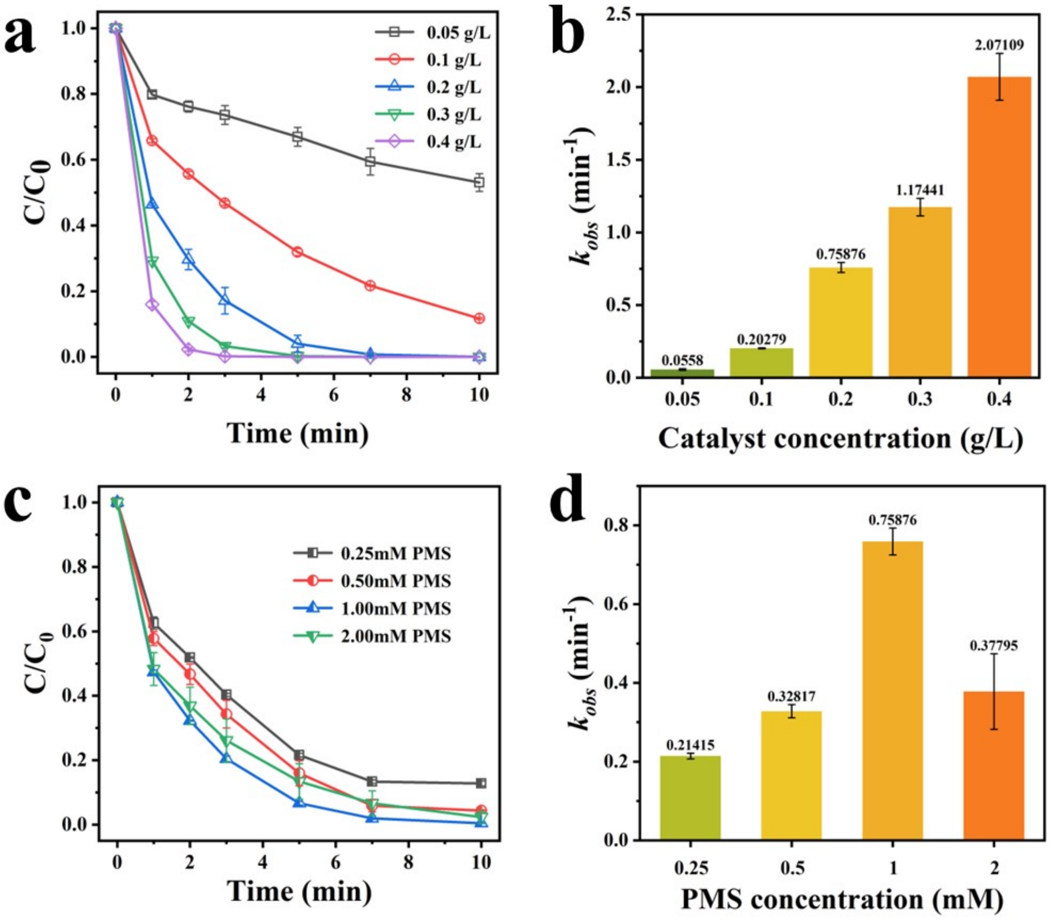

Fig. S19. The influence of (a-b) catalyst dosage, (c-d) PMS concentration on CBZ removal and corresponding k_{obs} values in the PANI-Fe@MoS$_2$ system.

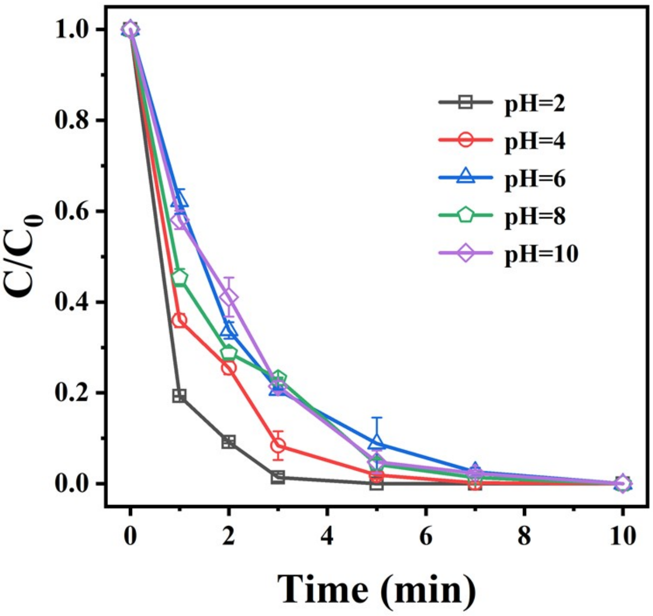

Fig. S20. The influence of pH on CBZ removal in the PANI-Fe@MoS$_2$ system.

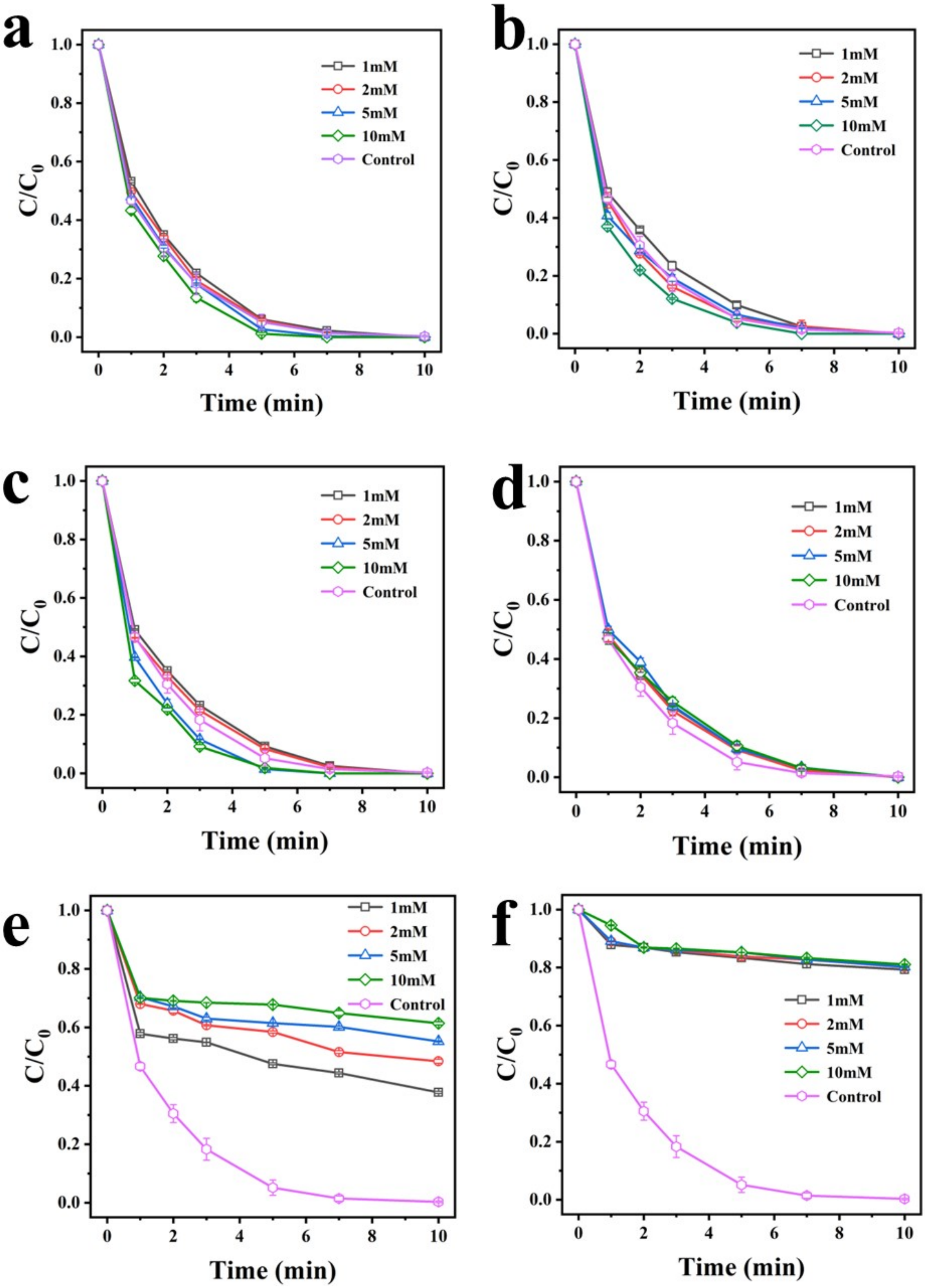

Fig. S21. CBZ removal with different concentrations of (a) Cl^-, (b) NO^{3-}, (c) NH_4^+, (d) SO_4^{2-}, (e) $H_2PO_4^-$, (f) HCO_3^- in the PANI-Fe@MoS$_2$ system.

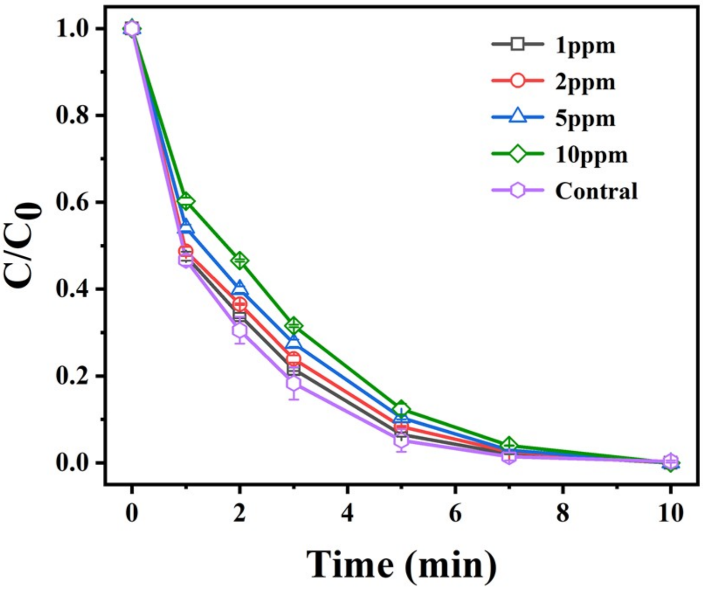

Fig. S22. The influence of humic acid with difference concentration.

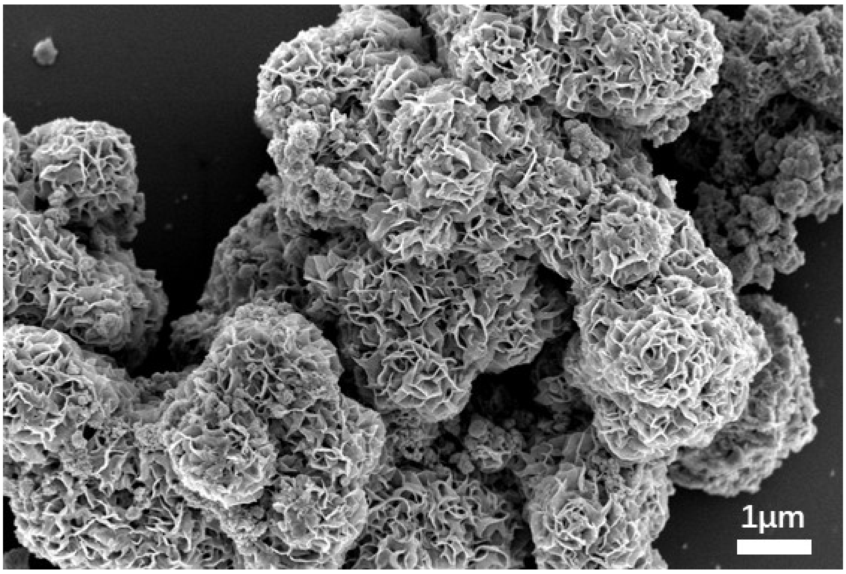

Fig. S23. The SEM images of used PANI-Fe@MoS_2.

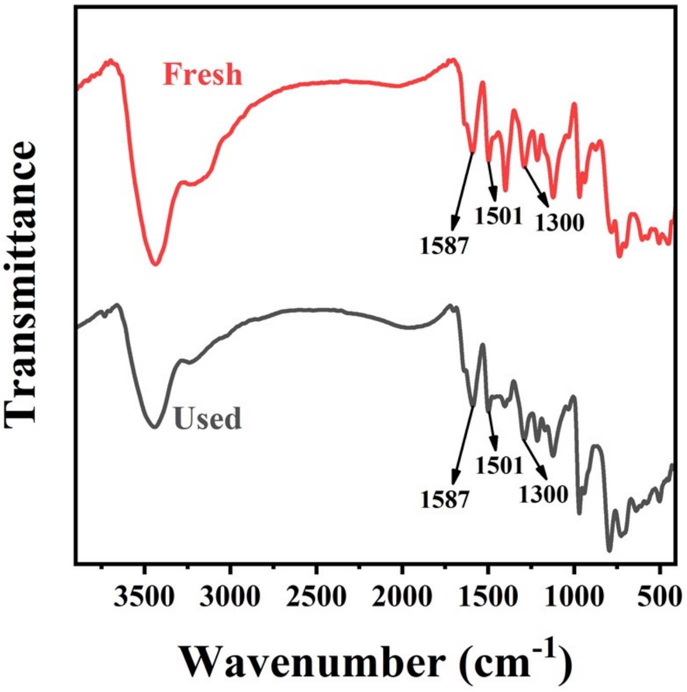

Fig. S24. FT-IR spectra of fresh PANI-Fe@MoS_2 and used PANI-Fe@MoS_2.

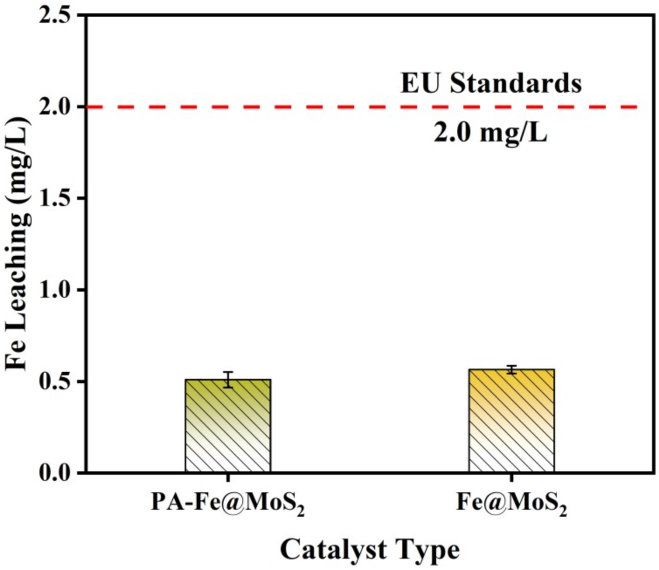

Fig. S25. The Fe leaching in the different systems**.**

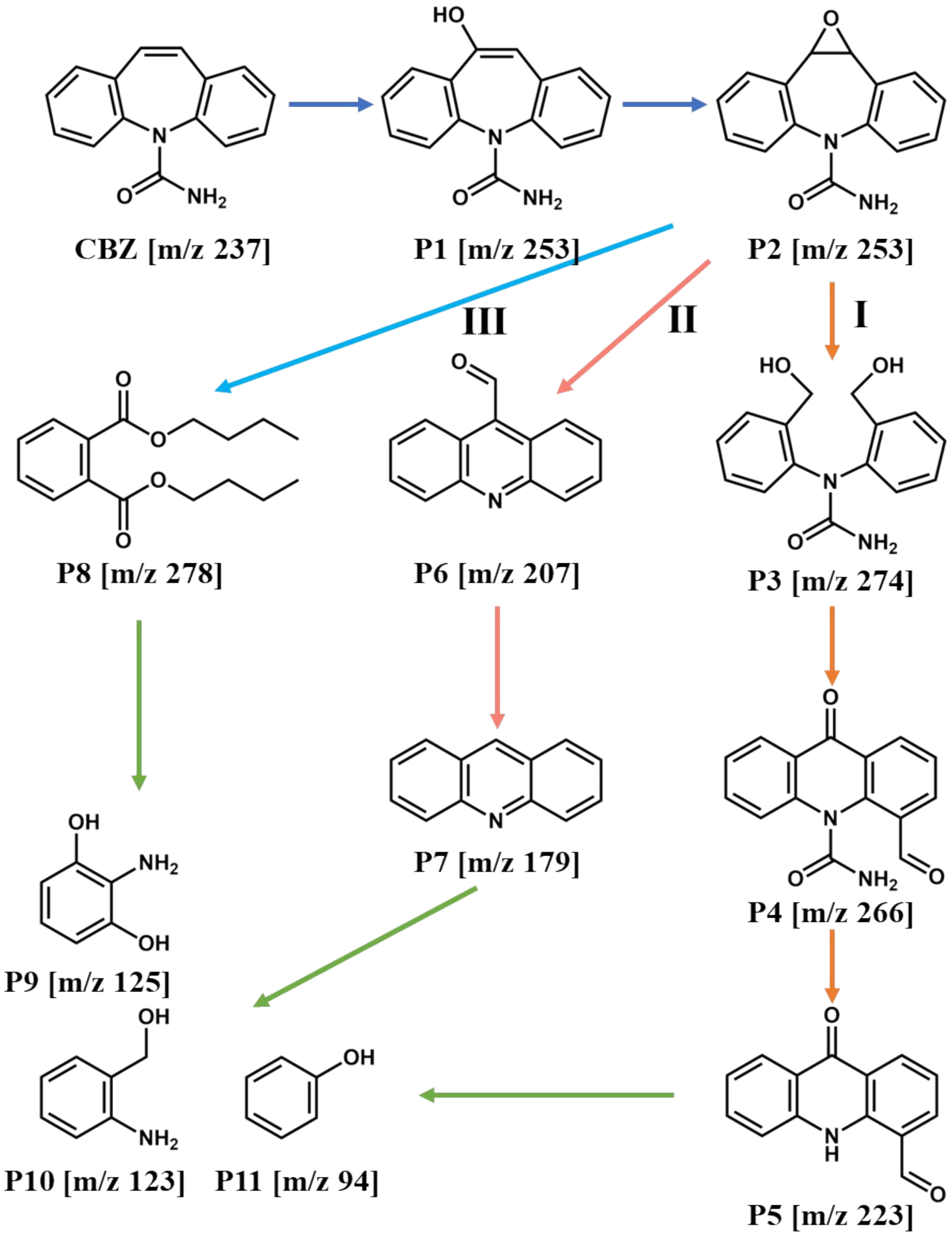

Fig. S26. Possible degradation pathways for CBZ

Table S1. Comparison of layer spacing with recently reported MoS_2 intercalation materials.

Catalyst	Layer spacing of MoS_2	Ref.
PANI-Fe@MoS_2	1.086nm	This work
MoS_2	0.62nm	1
PVP@MoS_2	0.68nm	2
oxygen-incorporated MoS_2	0.95nm	3
ET&IE MoS_2	0.94nm	4
MoS_2/CTAB	0.95nm	5
SDBS-MoS_2/BC	0.76nm	6
C-MoS_2	0.96nm	7
SDS-MoS_2	0.83nm	8

Table S2. Comparison of reaction parameters with recently reported heterogeneous catalysts for contaminant degradation.

Catalyst	Catalyst dose（g/L）	PMS concentration（mM）	CBZ concentration (mg/L)	Removal rate (reaction time)	k_{obs}	*k*-value	Ref.
PANI-Fe@MoS$_2$	0.20	1.00	23.63	100% 10min	0.75876	89.65	This work
MoS$_2$	0.20	0.60	5.01	95% 40min	0.074	3.09	9
CSWR-2	1.00	0.50	1.18	100% 30min	0.1606	0.38	10
Fe$_2$@BC$_{900℃}$	0.10	5.00	10.00	94.12% 20min	0.6574	13.15	11
FeS$_2$@C	0.10	0.65	10.00	98.6% 30min	0.2094	32.22	12
Fe/FeC$_3$@NC	0.15	1.62	10.00	100% 30min	0.622	25.59	13
Ru-LDH	0.10	0.65	23.63	100% 25min	0.118	42.90	14
Co-CCF-600	0.10	1	20.00	93.47% 60min	0.035	7	15
S$_{0.3}$-Co@P$_2$C	0.16	1.62	20.00	100% 15min	0.7445	57.45	16
CoCeO$_x$	0.02	0.12	2.00	98% 40min	0.078	65	17
CoSe$_{2-x}$@N - C - 500	0.2	3.25	10.00	100% 30min	0.25601	3.94	18
ZrO$_2$-C	0.10	0.04	2.36	95.2% 60min	0.0515	30.39	19
CoSBC-900	0.10	0.98	20.00	95.73% 20min	0.1287	26.27	20
NMS-10	0.40	0.98	5.00	71% 120min	0.00999	0.13	21
310-α-MnO$_2$	0.20	0.65	5.00	100% 30min	0.1663	6.40	22
N-CNT-2B	0.05	10.00	10.00	100% 60min	0.0677	1.35	23
HYSCN-8	0.06	0.40	5.00	96% 30min	0.108	22.5	24
FeS$_2$/WS$_2$	0.25	0.20	2.00	99% 40min	0.108	4.32	25
E @ MO	0.20	1.00	5.00	100% 60min	0.0622	1.56	26

Table S3. Comparison of chemical composition of PANI-Fe@MoS_2 in different stages.

Spectra	State	Before reaction	After reaction
Fe 2p	Fe (II)	56.48%	57.14%
	Fe (III)	43.52%	42.86%
Mo 3d	Mo (IV)	82.92%	80.54%
	Mo (VI)	17.08%	19.46%
N 1s	−N=	31.25%	24.60%
	−NH−	63.32%	73.32%
	$-N^+-$	5.43%	2.08%

Table S4. Comparison of chemical composition of Fe@MoS_2 in different stages.

Spectra	State	Before reaction	After reaction
Fe 2p	Fe (II)	51.52%	52.32%
	Fe (III)	48.48%	47.68%
Mo 3d	Mo (IV)	95.71%	95.25%
	Mo (VI)	4.29%	4.75%

Table S5. Degradation intermediates of CBZ detected by LC−MS.

Compound NO.	chemical formula	Molecular structure	MW [c]
P1	$C_{15}H_{12}O_2N_2$	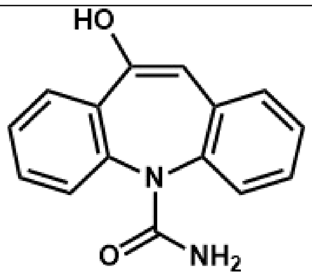	253
P2	$C_{15}H_{12}O_2N_2$	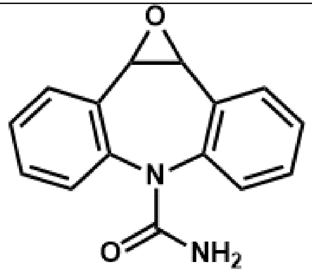	253
P3	$C_{15}H_{16}O_3N_2$	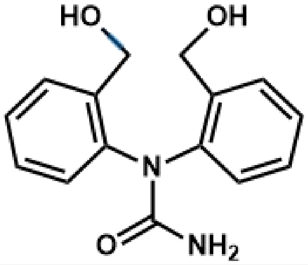	274
P4	$C_{15}H_{10}O_3N_2$	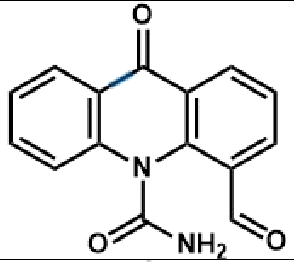	266
P5	$C_{14}H_{10}O_2N$	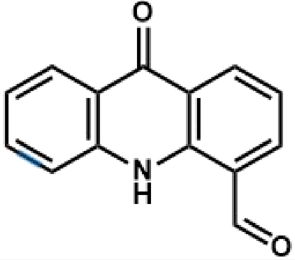	223
P6	$C_{14}H_9ON$	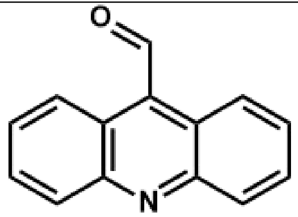	207

P7	$C_{13}H_9N$	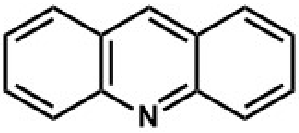	179
P8	$C_{16}H_{22}O_4$	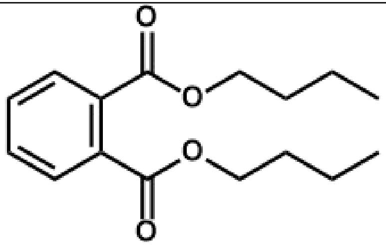	278
P9	$C_6H_7O_2N$	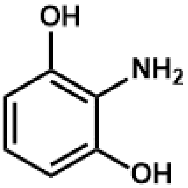	125
P10	C_7H_9ON	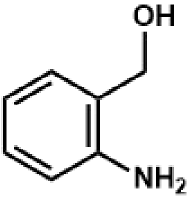	123
P11	C_6H_6O	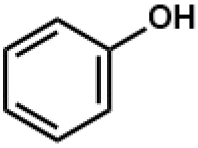	94

References

1. X. Zhang, Y. Jin, K. Zhang, Q. Yuan, H. Wang and M. Jia, *Journal of Colloid and Interface Science*, 2023, **630**, 786-794.
2. W. Wang, B. Qiu, C. Li, X. Shen, J. Tang, Y. Li and G. Liu, *Electrocatalysis*, 2020, **11**, 383-392.
3. J. Xie, J. Zhang, S. Li, F. Grote, X. Zhang, H. Zhang, R. Wang, Y. Lei, B. Pan and Y. Xie, *Journal of the American Chemical Society*, 2013, **135**, 17881-17888.
4. M.-R. Gao, M. K. Y. Chan and Y. Sun, *Nature Communications*, 2015, **6**.
5. W. Cai, D. D. Dionysiou, F. Fu and B. Tang, *Journal of Hazardous Materials*, 2020, **396**.
6. Y. Wang, X. Liu, X. Lin, H. Yuan, M. Liu and L. Zhang, *Chemical Engineering Journal*, 2024, **499**.
7. T. Yang, N. Gao and B. Li, *Bioresource Technology*, 2024, **401**.
8. J. Wang, R. Zhang, Y. Huo, Y. Ai, P. Gu, X. Wang, Q. Li, S. Yu, Y. Chen, Z. Yu, J. Chen and X. Wang, *Ecotoxicology and Environmental Safety*, 2019, **175**, 251-262.
9. H. Zhou, L. Lai, Y. Wan, Y. He, G. Yao and B. Lai, *Chemical Engineering Journal*, 2020, **384**.
10. C. Pan, Y. Sun, Y. Dong, H. Hou, M.-F. Kai and J. Lan, *Journal of Hazardous Materials*, 2024, **465**.
11. T. Wang, T. Zhang, M. Ta, J. Guo, R. Yang, J. Ren, Y. Zhen, C. Wang, C. Bai, C. Zhao and F. Zhang, *Separation and Purification Technology*, 2024, **328**.
12. C. Ma, Y. Liu, J. Wang, N. T. Evrard Deric, Y. Li, X. Fan and W. Peng, *Chemosphere*, 2024, **355**.
13. N. Li, J. Wang, T. Liao, B. Ma, Y. Chen, Y. Li, X. Fan and W. Peng, *Journal of Colloid and Interface Science*, 2024, **672**, 688-699.
14. Y. Tan, Z. Yang, C. Zhang, Y. Huang, Y. Li, K. Yang and Q. Long, *Separation and Purification Technology*, 2024, **349**.
15. Y. Li, Q. An, Z. Xiao, K. Zhu, X. Zhang, C. Wang, Y. Liu and S. Zhai, *Chemical Engineering Journal*, 2024, **487**.
16. H. Jiang, J. Zhou, Q. Zhou, L. Qin, D. Zhao, H. Liu, M. Yang and Y. Zhang, *Chemical Engineering Journal*, 2024, **489**.

17. S. Kang, Y. Ren, C. Liu, N. Li, B. Lai and J. Li, *Chemical Engineering Journal*, 2024, **494**.

18. T. Liao, X. Liu, Y. Liu, N. Li, J. Wang, N. Li, X. Wang, Y. Li, X. Fan and W. Peng, *Journal of Colloid and Interface Science*, 2024, **665**, 219-231.

19. X. Li, J. Liu, R. Lv, Y. Chu, L. Lv, J. Lu and W. Zhang, *Chemical Engineering Journal*, 2023, **463**.

20. X. Peng, Y. Li, K. Zhu, Q. An, J. Hao, Z. Xiao, X. Dong and S. Zhai, *Journal of Environmental Chemical Engineering*, 2023, **11**.

21. W. Liu, Y. Yang, Y. Li, Y. Zhou, C. Wang, Y. Zhou, J. Shang and X. Cheng, *Separation and Purification Technology*, 2024, **329**.

22. H. Wei, J. Zhao, B. Shang and J. Zhai, *Journal of Environmental Chemical Engineering*, 2022, **10**.

23. S. Liu, Q. Pan, J. Li, M. Wang, J. Zhang, Y. Song, C. Zhao, J. Shi and H. Deng, *ACS ES&T Water*, 2022, **2**, 817-829.

24. Z. Wu, Z. Xiong, R. Liu, C. He, Y. Liu, Z. Pan, G. Yao and B. Lai, *Journal of Hazardous Materials*, 2022, **427**.

25. G. Gou, S. Kang, H. Zhao, C. Liu, N. Li, B. Lai and J. Li, *Separation and Purification Technology*, 2022, **290**.

26. L. Zhu, Z. Shi, L. Deng, J. Chen and H. Zhang, *Process Safety and Environmental Protection*, 2022, **158**, 42-54.